Flux through hepatic pyruvate carboxylase and phosphoenolpyruvate carboxykinase detected by hyperpolarized ^{13}C magnetic resonance

Matthew E. Merritt[a,b,c,1], Crystal Harrison[a], A. Dean Sherry[a,c,d,e], Craig R. Malloy[a,b,c,d,f], and Shawn C. Burgess[a,g,1]

[a]Advanced Imaging Research Center, [b]Department of Molecular Biophysics, [c]Department of Radiology, [f]Department of Internal Medicine, and [g]Department of Pharmacology, University of Texas Southwestern Medical Center, Dallas, TX 75390-8568; [d]Veterans Affairs North Texas Healthcare System, Dallas, TX 75216-7167; and [e]Department of Chemistry, University of Texas at Dallas, Richardson, TX 75216-7167

In the heart, detection of hyperpolarized [^{13}C]bicarbonate and ^{13}CO$_2$ by magnetic resonance (MR) after administration of hyperpolarized [1-^{13}C]pyruvate is caused exclusively by oxidative decarboxylation of pyruvate via the pyruvate dehydrogenase complex (PDH). However, liver mitochondria possess alternative anabolic pathways accessible by [1-^{13}C]pyruvate, which may allow a wider diagnostic range for hyperpolarized MR compared with other tissue. Metabolism of hyperpolarized [1-^{13}C]pyruvate in the tricarboxylic acid (TCA) cycle was monitored in the isolated perfused liver from fed and fasted mice. Hyperpolarized [1-^{13}C]pyruvate was rapidly converted to [1-^{13}C]lactate, [1-^{13}C]alanine, [1-^{13}C] malate, [4-^{13}C]malate, [1-^{13}C]aspartate, [4-^{13}C]aspartate, and [^{13}C] bicarbonate. Livers from fasted animals had increased lactate:alanine, consistent with elevated NADH:NAD$^+$. The appearance of asymmetrically enriched malate and aspartate indicated high rates of anaplerotic pyruvate carboxylase activity and incomplete equilibration with fumarate. Hyperpolarized [^{13}C]bicarbonate was also detected, consistent with multiple mechanisms, including cataplerotic decarboxylation of [4-^{13}C]oxaloacetate via phosphoenolpyruvate carboxykinase (PEPCK), forward TCA cycle flux of [4-^{13}C] oxaloacetate to generate ^{13}CO$_2$ at isocitrate dehydrogenase, or decarboxylation of [1-^{13}C]pyruvate by PDH. Isotopomer analysis of liver glutamate confirmed that anaplerosis was sevenfold greater than flux through PDH. In addition, signal from [4-^{13}C] malate and [4-^{13}C]aspartate was markedly blunted and signal from [^{13}C]bicarbonate was completely abolished in livers from PEPCK KO mice, indicating that the major pathway for entry of hyperpolarized [1-^{13}C]pyruvate into the hepatic TCA cycle is via pyruvate carboxylase, and that cataplerotic flux through PEPCK is the primary source of [^{13}C]bicarbonate. We conclude that MR detection of hyperpolarized TCA intermediates and bicarbonate is diagnostic of pyruvate carboxylase and PEPCK flux in the liver.

dynamic nuclear polarization | metabolic flux | gluconeogenesis

Hepatic metabolism is comprised of a network of exergonic reactions that facilitate energy capture, such as fatty acid oxidation, carbohydrate oxidation and flux through the tricarboxylic acid (TCA) cycle, and endergonic reactions required for gluconeogenesis, lipogenesis, and amino acid biosynthesis. The dysregulation of these pathways underlie the pathology of a variety of diseases, including diabetes, cancer, and inborn errors of metabolism, making their diagnostic evaluation critically important. In particular, the hepatic TCA cycle is an important diagnostic target because its intermediates integrate lipid, carbohydrate, and amino acid metabolism during normal physiology. As examples, oxaloacetate is the common intermediate by which all noncarbohydrate sources enter gluconeogenesis; citrate is required to shuttle acetyl-CoA from the mitochondria for cytosolic lipogenesis; and the ketoacids of the TCA cycle serve as intermediates of amino acid synthesis and catabolism. The interconnectivity of these hepatic pathways makes their examination difficult but worthwhile because technologies that detect

these fluxes provide important advances for basic and clinical investigation of mechanisms of disease.

Dynamic nuclear polarization (DNP) of ^{13}C is a powerful molecular imaging technology that uses principles of magnetic resonance (MR) (1). Prepolarization of ^{13}C-labeled tracers enhances the sensitivity of MR by 10,000-fold or more and enables studies of cancer (2), hepatic metabolism (3, 4), and cardiac metabolism (5–7). In the heart, metabolism of hyperpolarized [1-^{13}C]pyruvate to ^{13}CO$_2$ and [^{13}C]bicarbonate is caused exclusively by flux through the pyruvate dehydrogenase complex (PDH). Consequently, ^{13}CO$_2$ detection is not necessarily indicative of flux in the TCA cycle, because non-PDH sources of acetyl-CoA (e.g., fat oxidation) dominate the metabolism of certain tissues, like the liver. Recently, DNP was used to observe altered cytosolic redox state in liver following ethanol administration (3), and hyperpolarized bicarbonate was observed in vivo after administration of [1-^{13}C]lactate, but analysis of oxidative versus biosynthetic metabolism in the liver has not been reported. In contrast to the heart, hepatic anaplerosis is four- to sixfold higher than acetyl-CoA oxidation (8–10). Consequently, the appearance of hyperpolarized [^{13}C]bicarbonate could indicate flux in multiple alternative pathways, including direct decarboxylation of [1-^{13}C]pyruvate by PDH, anaplerotic carboxylation of [1-^{13}C]pyruvate followed by equilibration with TCA cycle intermediates, and subsequent cataplerotic decarboxylation of [4-^{13}C]oxaloacetate via phosphoenolpyruvate carboxykinase (PEPCK) or flux of [1-^{13}C]oxaloacetate into citrate followed by downstream oxidative decarboxylation in the TCA cycle.

Here, we demonstrate that hyperpolarized [1-^{13}C]pyruvate may be used to detect flux in both anaplerotic and cataplerotic reactions in the liver. The appearance of hyperpolarized [1-^{13}C] malate, [1-^{13}C]aspartate and smaller amounts of [4-^{13}C]malate and [4-^{13}C]aspartate detected metabolism of [1-^{13}C]pyruvate into the TCA cycle via pyruvate carboxylase enzyme within seconds after administration of hyperpolarized [1-^{13}C]pyruvate, followed by rapid but incomplete "backwards" equilibration with the symmetric intermediate, fumarate. The polarization profiles of these hepatic metabolites changed as anticipated during feeding and fasting. Signal from hyperpolarized [^{13}C]bicarbonate was also observed. A ^{13}C isotopomer analysis of glutamate isolated from separate livers demonstrated that flux through PEPCK is ~sevenfold higher than flux through PDH, indicating that flux through PEPCK may be a significant source of the

www.manaraa.com

hyperpolarized [^{13}C]bicarbonate detected in the liver. To further confirm the metabolic source of [^{13}C]bicarbonate, livers that do not express PEPCK (9, 11) were examined. PEPCK loss of function completely abolished [^{13}C]bicarbonate production and substantially blunted the appearance of label in the 4-carbon intermediates of the TCA cycle, indicating that hyperpolarized [^{13}C]bicarbonate results from PEPCK activity in the liver. These findings broaden the diagnostic scope of hyperpolarized MR to include liver pathways previously inaccessible by in vivo imaging modalities.

Results

Hyperpolarized ^{13}C MR Provides Real-Time Detection of Multiple Enzymatic Reactions.

Although pyruvate oxidation is minimal in the liver, it serves as a vital synthetic precursor for a variety of metabolites, most notably glucose. Because hepatic gluconeogenesis is critical for normal glucose homeostasis, we determined whether the fate of hyperpolarized [1-^{13}C]pyruvate could be used to monitor the anaplerotic reaction of pyruvate carboxylase, which converts pyruvate into oxaloacetate in liver mitochondria. Oxygen consumption in perfused livers was 1.26 μmol/gww/min, similar to earlier reports (9), indicating normal hepatic function. The sum of the first 60 ^{13}C spectra obtained following the initial observation of the [1-^{13}C]pyruvate signal demonstrated generation of a variety of metabolites from [1-^{13}C]pyruvate (Fig. 1). Metabolites derived from pyruvate in a single cytosolic enzyme-catalyzed step, such as lactate and alanine, had the largest peak intensities in all spectra, similar to observations in other tissues (7, 12). As expected, fasted livers (Fig. 1, *Middle*) had high lactate/alanine polarization ratios compared with fed livers (Fig. 1, *Bottom*), reflecting the known decrease in cellular redox state associated with fasting (13). In addition to lactate and alanine, resonances associated with two 4-carbon metabolites, malate and aspartate, were also observed, with labeling apparent at both the C1 and C4 positions. Because there are no previous reports of these metabolites in hyperpolarized ^{13}C studies, we confirmed the assignments in tissue extracts using thermally polarized liquid-state ^{13}C NMR and heteronuclear multiple bond coherence 2D ^{1}H-^{13}C correlation spectroscopy (see *SI Text*). Because of the crowding present in the carbonyl region of the spectrum of the hyperpolarized species, it is impossible to definitively exclude the presence of other metabolites, such as [1-^{13}C]fumarate, which would be expected to be close to the [1-^{13}C]aspartate resonance, and either [6-^{13}C] or [1-^{13}C]citrate, which would be close to the [1-^{13}C]malate and pyruvate-hydrate signals, respectively. However, we believe our assignments to be accurate. The appearance of these TCA cycle intermediates signified the rapid carboxylation of pyruvate to oxaloacetate (pyruvate carboxylase flux), an observation that is distinct from previous hyperpolarization experiments in the heart and other tissues where this pathway is insignificant. Hepatic pyruvate carboxylase is the first enzymatic step in the conversion of pyruvate to glucose and certain amino acids and is also critical to replenish mitochondrial oxaloacetate lost to other processes, such as lipogenesis. Surprisingly, the appearance of these intermediates was similar in both fed and fasted livers (Fig. 1, *Bottom* and *Middle*), indicating sustained activity of pyruvate carboxylation regardless of nutritional state. To confirm that polarization of malate and aspartate is the result of anaplerosis, we examined livers lacking PEPCK expression. These livers cannot synthesize glucose from pyruvate and have severely impaired rates of pyruvate carboxylase flux (9). As expected, polarization of malate and aspartate was considerably blunted but not completely eliminated in livers lacking PEPCK (Fig. 1, *Top* and Fig. 2, *Right*). These data demonstrate that ^{13}C MR detection of malate and aspartate following hyperpolarized [1-^{13}C]pyruvate administration is an indicator of pyruvate carboxylase flux in liver.
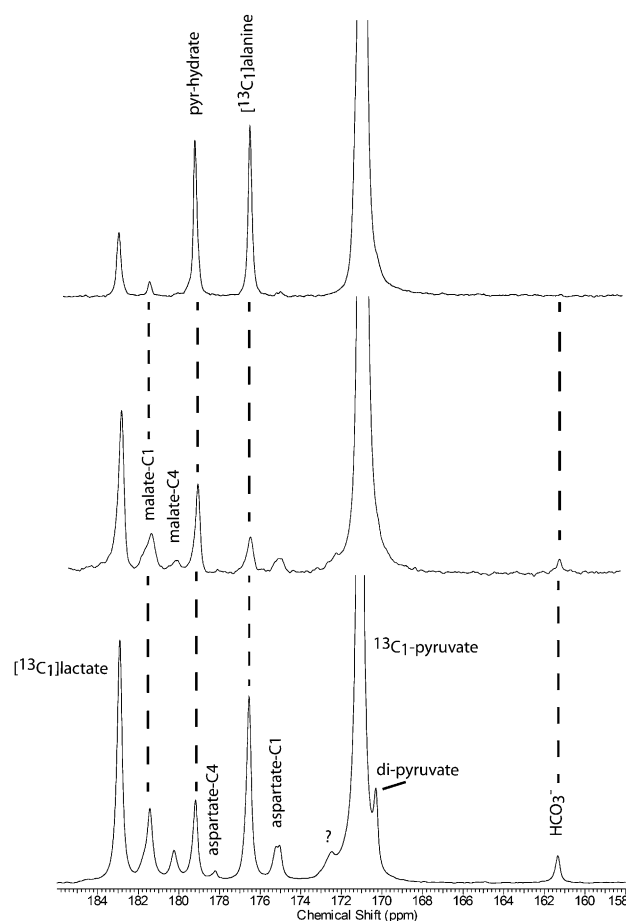

Fig. 1. ^{13}C spectra derived from the sum of 60 scans following the injection of HP [1-^{13}C]pyruvate into a perfused liver excised from a fed (*Bottom*), fasted (*Middle*), or PEPCK knockout mouse (*Top*). No resonance for ^{13}CO$_2$ were observed at 125 ppm. The pyruvate-hydrate signal at 179 ppm is always present as an impurity in the spectrum of pyruvate, but the di-pyruvate signal upfield of the [1-^{13}C]pyruvate signal is only occasionally observed.

Malate and Aspartate Signals Indicate Backward Exchange in the TCA Cycle.

Because malate is an intermediate of the TCA cycle and aspartate is in rapid exchange with oxaloacetate, we examined the temporal characteristics of their signals to determine whether insight into TCA cycle dynamics could be obtained. The ^{13}C signals from all detected metabolites as a function of time are shown in Fig. 2 ($n = 4$ for each). The hyperpolarized (HP) lactate and alanine signals in spectra of fed livers (Fig. 2, *Left*) were larger than those assigned to the C1 and C4 of malate and aspartate at all time points, and the lactate and alanine signal intensities roughly paralleled one another. The ratios [4-^{13}C] malate/[1-^{13}C]malate and [4-^{13}C]aspartate/[1-^{13}C]aspartate were ~33%, demonstrating that a significant fraction of [1-^{13}C]oxaloacetate, derived from carboxylation of [1-^{13}C]pyruvate, must have entered the fumarate pool, a symmetric intermediate. Bicarbonate was the smallest of all of the resonances, contributing only ~0.02% of the total carbon signal at maximum intensity. Differences between normalized ^{13}C resonance amplitudes for the fasted livers compared with fed livers are readily discernable in Fig. 2, *Center*. The peak [1-^{13}C]lactate signal is slightly lower for the fasted liver, but [1-^{13}C]alanine is much lower, actually falling below the level of [1-^{13}C]malate. The signal of [1-^{13}C] aspartate is also small compared with the [1-^{13}C]malate signal, but [4-^{13}C]aspartate is not observable in the spectra as a function

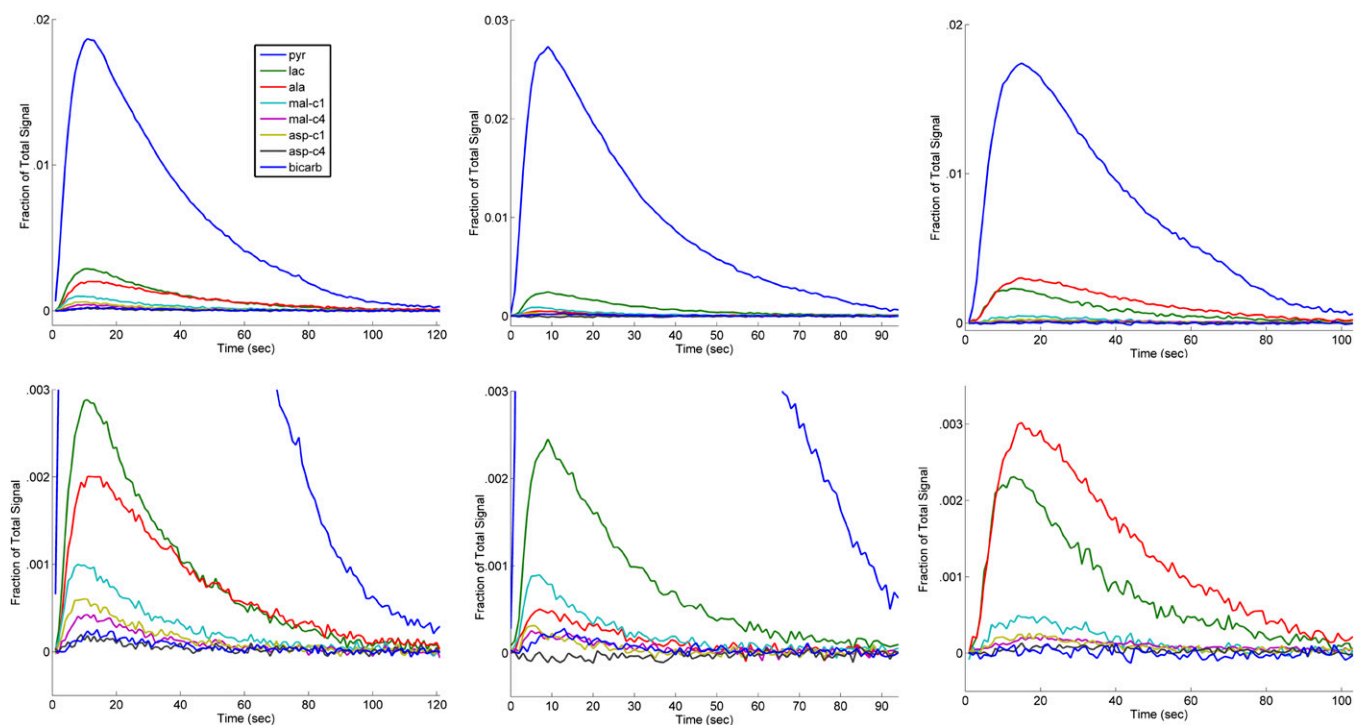APPLIED PHYSICAL SCIENCES

SYSTEMS BIOLOGY

Fig. 2. Integrated, scaled intensities for the metabolites observed in the fed (*Left*), fasted (*Center*), and PEPCK knockout (*Right*) mouse liver as a function of time following injection of 2 mM HP [1-^{13}C]pyruvate. The total signal was obtained by summing over all of the resonances of pyruvate and its metabolites. Note that the fraction of signal in the metabolites of [1-^{13}C]pyruvate in the fasted liver is lower than for the fed animals. The PEPCK knockout animals showed lower intensities for the TCA cycle metabolites versus the fed animal, and no [^{13}C]bicarbonate.

of time, with only a small resonance visible in the summed spectra (Fig. 1, *Middle*).

The ratio of ^{13}C enrichment in positions 1 and 4 of the 4-carbon intermediates, malate and aspartate, provides insight into the exchange reactions that share oxaloacetate as a common intermediate. Appearance of ^{13}C at the C1 position of aspartate or malate occurs as a direct result of carboxylation of [1-^{13}C]pyruvate to produce [1-^{13}C]oxaloacetate. Reduction of [1-^{13}C]oxaloacetate produces only [1-^{13}C]malate. However, further reaction to the symmetric intermediate fumarate results in the repositioning of 50% of the label into each of the C1 and C4 positions. The ratio of these two peaks should therefore contain information about the kinetics of the malate-fumarate equilibrium (14). The appearance of ^{13}C label at the C1 positions of malate and aspartate occur almost instantaneously, but its appearance at the C4 position lagged by ~2 s because of the temporal delay for the metabolites to proceed to fumarate and back into the malate, oxaloacetate, and aspartate pools. If the average T$_1$s of the carboxyl carbons is 12 s, then the expected loss of intensity in the C4-positions would be ~15% compared with the C1 positions on the first pass through fumarate. Ratios were calculated excluding the times where they were still changing rapidly (immediately following the injection) and where the signal-to-noise for the C4-enriched metabolites decreased to an immeasurably low level (late). The average ratio [4-^{13}C]malate/[1-^{13}C]malate was 0.41 ± 0.06 in fed livers but 0.29 ± 0.08, ($P =$ 4.6e^{-9}) in fasting livers, indicating that symmetrization at the level of fumarate is slower in the fasted state, perhaps reflecting increased TCA cycle turnover or gluconeogenesis during fasting. Because the T$_1$s of the C1 and C4 position are so similar, comparing the ratio of C4 to C1 between the fed and fasted state should not be unduly weighted by the longitudinal relaxation. Similarly, the aspartate observed in these spectra was derived from oxaloacetate (by the action of aspartate amino transferase)

and the ratio [4-^{13}C]aspartate/[1-^{13}C]aspartate for the fed animals was 0.27 ± 0.09 compared with a ratio of essentially zero throughout in fasted livers, as [4-^{13}C]aspartate was not observed. Aspartate labeled at the C4 position must necessarily have been derived from oxaloacetate that has cycled back to fumarate, then forward again to make aspartate. These data suggest that in addition to the appearance of malate and aspartate as an indicator of pyruvate carboxylase activity, the backward exchange of those metabolites are detectable in the randomization of C1 and C4, providing additional information about TCA cycle dynamics or cataplerosis of oxaloacetate or malate (15).

Bicarbonate Generation Indicates Cataplerotic Activity in the Liver. Generation of hyperpolarized [^{13}C]bicarbonate subsequent to the decarboxylation of [1-^{13}C]pyruvate has been used as an indicator of PDH flux in the heart and other tissues (7). Liver is thought to have relatively minor rates of PDH flux, but HP bicarbonate nevertheless appeared in both fed and fasted liver at 161 ppm in the spectra (Fig. 1, *Middle* and *Bottom*). The appearance of HP [^{13}C]bicarbonate in the liver could arise from some combination of four reactions: (*i*) flux of [1-^{13}C]oxaloacetate "backward" into fumarate followed by generation of [4-^{13}C]oxaloacetate and decarboxylation via PEPCK; (*ii*) a similar process that generates [4-^{13}C]malate followed by decarboxylation via the malic enzyme; (*iii*) flux of [1-^{13}C]oxaloacetate "forward" through citrate synthase with generation of HP bicarbonate at the isocitrate dehydrogenase reaction; or (*iv*) flux through pyruvate dehydrogenase. The first three possibilities require flux through pyruvate carboxylase but the latter possibility does not. To determine the relative contribution of PDH and pyruvate carboxylase pathways to the incorporation of pyruvate carbons into the TCA cycle, the source of the [^{13}C] bicarbonate signal was evaluated using classic steady-state ^{13}C isotopomer analysis (16). Livers from fed animals were perfused

to steady state with [U-^{13}C]pyruvate, but with conditions that were otherwise identical to the HP experiments. Isotopomer analysis of glutamate in tissue extracts (17) indicated the ratio of pyruvate carboxylase/PDH flux was 7.6 ± 2.0, demonstrating that the great majority of pyruvate entry into the TCA cycle was via pyruvate carboxylase rather than PDH. A small flux of [U-^{13}C]pyruvate through PDH was detected; the fraction of the acetyl-CoA pool derived from [U-^{13}C]pyruvate ([1,2-^{13}C]acetyl CoA) was 7 ± 3%. Thus, although PDH flux from pyruvate was very small, hyperpolarized [^{13}C]bicarbonate could be generated.

To assess whether detection of HP bicarbonate indicates cataplerotic activity in the liver, we again evaluated bicarbonate generation in mice lacking hepatic PEPCK. The effects of PEPCK knockout are shown in the fractional resonance amplitudes in Fig. 2 (*Right*) and in Fig. 3. The cytosolic metabolites lactate and alanine are elevated relative to the 4-carbon metabolites. The small resonance assigned as [1-^{13}C]aspartate was detected in only one of four spectra, but the HP-bicarbonate signal was not detected in any of the spectra from this group (Fig. 1, *Top*). These data indicate that the appearance of HP bicarbonate is caused primarily by flux through pyruvate carboxylation followed by cataplerotic decarboxlation, most likely at the PEPCK step.

Discussion

Previous studies of metabolism in the liver using HP [1-^{13}C]pyruvate or [1-^{13}C]lactate have detected HP [1-^{13}C]alanine and [1-^{13}C]lactate (3, 4). Therefore, the additional resonances observed for the perfused mouse liver shown in Fig. 1 was an unexpected finding. Previous results using HP [1-^{13}C]pyruvate to study the in vivo rat liver in the fed and fasted state were obtained using a surface coil at an MRI field strength of 3T (4). Despite the high sensitivity of the DNP experiment, TCA cycle intermediates were not observed in the in vivo rat liver. One notable difference in the experimental protocols was the use of a 5° excitation pulse for the previous work, which would yield lower signal-to-noise but would also permit increased time to observe the HP species compared with the larger flip angles used here. Few data are available comparing the relative metabolite levels in rat versus mouse liver, but it is also possible that malate and aspartate concentrations or dynamics are different between the species.

Source of [^{13}C]bicarbonate in the Perfused Liver. The detection of HP [^{13}C]bicarbonate in the liver (Figs. 1–3) is also strikingly different from previous reports by Spielman (3) and Hu (4). This difference is almost certainly related to the aforementioned lack of signal in TCA cycle intermediates in previous studies, because we conclude that the HP bicarbonate originates largely from anaplerosis/cataplerosis rather than PDH activity (Fig. 4). The preference for pyruvate carboxylase flux over PDH flux in the liver has been detected by ^{13}C NMR before using standard isotopomer methods (18). However, we investigated the source of HP [^{13}C]bicarbonate because it may provide diagnostic insight into key pathways, such as gluconeogenesis by detecting flux through pyruvate carboxylase and PEPCK. It is important to note that carboxylation of [1-^{13}C]pyruvate produces [1-^{13}C]oxaloacetate and if this product was converted to PEP directly via PEPCK, this would not produce ^{13}CO$_2$ or [^{13}C]bicarbonate. Thus, production of HP ^{13}CO$_2$ at the level of PEPCK could only occur after [1-^{13}C]oxaloacetate first exchanges with malate and fumarate pools to form [4-^{13}C]oxaloacetate. The asymmetry in ^{13}C enrichment of malate and aspartate reported here confirms that this process is active but incomplete at the timescale of the HP experiments in both fed and fasted livers. Previous work using ^{14}C radioisotopes reported complete equilibration between the oxaloacetate and fumarate pools, but the time scale of those experiments was in hours (15); the experiment reported here observed metabolic exchange on the order of seconds. A second possible pathway is flux of [1-^{13}C]oxaloacetate through citrate synthase, aconitase and isocitrate dehydrogenase. However, the fact that flux through pyruvate carboxylase is ~fivefold greater than TCA cycle flux implies that a weighted average of the sources of production for the [^{13}C]bicarbonate should favor the anaplerotic pathway. In agreement with this finding, despite a relatively high concentration of citrate in liver we did not detect any signal from [6-^{13}C] citrate, which should have been generated by [1-^{13}C]pyruvate, (Fig. 4). Similarly, the third possible pathway for bicarbonate generation—flux through PDH—was small relative to citric acid cycle flux, as determined by isotopomer analysis. Taken together, the experiments with fed and
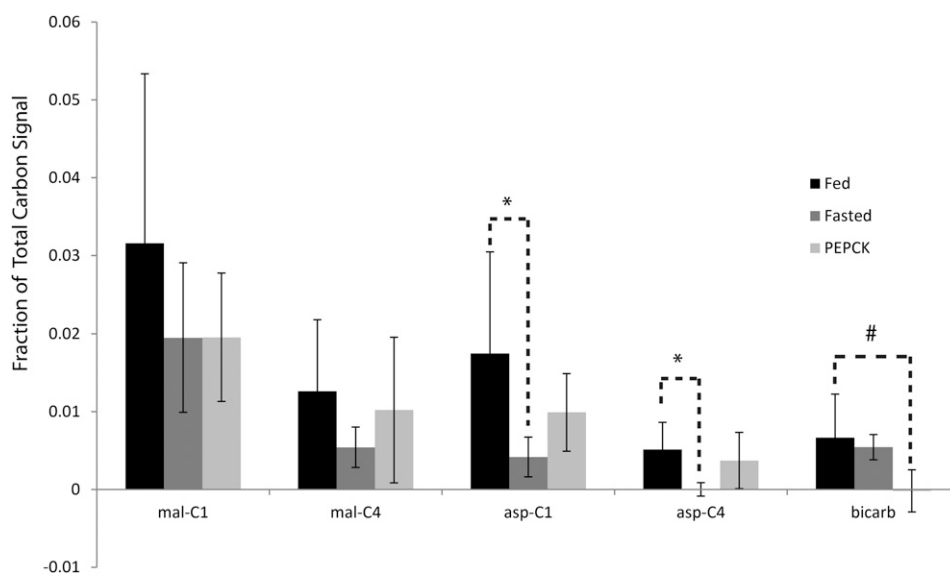

Fig. 3. The bar graph for the relative total carbon intensities comparing the fed, fasted, and PEPCK knockout livers. Asterisks (*) mark the metabolites that showed a significant difference in the integrated signal intensities between the fed and fasted case. The pound sign (#) denotes a significant difference between the fed animals and the PEPCK knockout. The large fractional amplitudes for the pyruvate, lactate, and alanine are omitted for clarity.
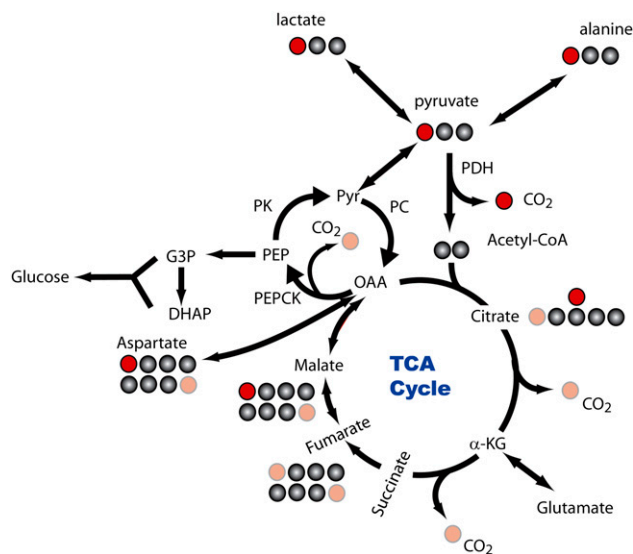
www.manaraa.com

Fig. 4. The introduction of [1-^{13}C]pyruvate leads to labeling at the C1 of lactate and alanine (red circles). If PDH flux is present, CO_2 can also be labeled. If pyruvate carboxylase flux is significant, label can appear at the C1 of malate. If the label is symmetrically distributed by the exchange between malate and fumarate, then it can also appear at the 4 position of various metabolites (red, semitransparent circles). CO_2 can be eliminated by the action of either PEPCK on the C4 position of oxaloacetate or by enzymatic reactions in the forward span of the TCA cycle. Labeling of the CO_2 in these cases depends upon the level of symmetrization achieved by the malate to fumarate exchange.

fasted animals plus the ^{13}C NMR isotopomer analysis indicate that the primary source of [^{13}C]bicarbonate is flux through pyruvate carboxylase followed by equilibration in fumarate and subsequent flux through PEPCK, although a related possibility might involve decarboxylation via the malic enzyme, which converts malate to pyruvate. The absence of [^{13}C]bicarbonate in livers from mice that do not express PEPCK is a strong indication that PEPCK flux is required for detection of the [^{13}C] bicarbonate signal; however, production through a forward turn of the TCA cycle cannot be completely excluded by the current experiments.

If [^{13}C]bicarbonate generation is associated with PEPCK flux, then the detection of [^{13}C]bicarbonate might qualitatively index gluconeogenesis. However, complications arise because of the number of enzymatic steps necessary for production of $^{13}CO_2$ following pyruvate carboxylation. It is also notable that 50–75% of PEPCK flux is cycled back to the TCA cycle (i.e., pyruvate cycling) rather than supporting gluconeogenesis (8–10, 18). Indeed, the lack of statistical significance between [^{13}C]bicarbonate production in the fed and fasted states (Fig. 3) suggests that further work will be required to evaluate hyperpolarized $^{13}CO_2$ as a metric of gluconeogenesis. Nonetheless, an increase in [^{13}C] bicarbonate production caused by coordinate up-regulation of the pyruvate carboxylase/PEPCK pathway during diseases like diabetes is a pathologic event now within the analytical scope of DNP.

Detection of Hyperpolarized ^{13}C Malate and Aspartate. The other difference between the current results and earlier reports (3, 4) was the observation of HP [1-^{13}C]malate, [1-^{13}C]aspartate, [4-^{13}C]malate and [4-^{13}C]aspartate. These observations are important because they demonstrate the ability to monitor downstream metabolites of [1-^{13}C]pyruvate through as many as six enzyme-catalyzed reactions (Fig. 4). The rate of exchange between oxaloacetate and fumarate has been studied previously

with ^{14}C tracers, and was found to be ~six-times the TCA cycle flux in humans (15). Consistent with this previous report, we found that malate and aspartate showed labeling in the C4 position, which is indicative of symmetrization of the label at the level of fumarate in the TCA cycle. The lack of complete equalization of the C1 and C4 does not necessarily contradict high rates of exchange between oxaloacetate and fumarate; rather, it reflects the rapid sampling of enrichment provided by hyperpolarized MR, which is not possible by sampling blood or urine steady-state metabolite enrichment. Because pyruvate carboxylation is considered the first step of gluconeogenesis in the liver, a potential explanation for the lower symmetrization in the fasted state is that flux through PEPCK is higher, and therefore oxaloacetate has less time to equilibrate with malate and fumarate before it is shunted to phosphoenolpyruvate and ultimately to glucose. This explanation also agrees with the observations of lower total carbon counts in the metabolites in the fasted state. Increased flux through PEPCK (and subsequently through enolase to make 2-P-D-glycerate in the route to glucose) may inhibit oxaloacetate from being cycled back to malate and fumarate, a kinetic effect. This interpretation, however, could be offset by the fact that the equilibrium pool sizes of malate and aspartate are smaller in the fasted state and this would result in smaller signals detected for these metabolites, a thermodynamic effect. Yang, et al., previously described the exchange of ^{13}C label between malate and aspartate in vivo using a set of modified Bloch equations that did not take into account the effects of relaxation in the substrate-enzyme complex (19). With the caveats laid out in the results section regarding the T_1 relaxation of the C1 and C4 positions of both malate and aspartate, we believe that ratios of C4 to C1 labeling in the fed and fasted state are accurate to within 15%. Interestingly, the pool size of malate is ~10-times larger in PEPCK knockout livers (9), so HP malate and aspartate in principle should have been more readily detected. Alternatively, because PEPCK (the dominant cataplerotic pathway in liver) is absent in these livers, carboxylation of [1-^{13}C]pyruvate to form [1-^{13}C]oxaloacetate is also severely blunted. Either mechanism or some combination would explain the observed differences between the three groups of livers examined here.

Relevance of DNP for Analysis of Hepatic Metabolism. The appearance of asymmetric ^{13}C labeling in malate and aspartate, and the detection of [^{13}C]bicarbonate provides direct information about pyruvate carboxylation in the intact liver. In view of the many metabolic complications associated with liver disease, including nonalcoholic fatty liver disease, hepatitis, cirrhosis, and diabetes, a method for assessing in vivo hepatic metabolism that does not require a biopsy, radiation, or lengthy tracer infusion procedures represents an important advance in medical diagnostics, especially because HP approaches has been translated to humans. With the proliferation of mouse models for human disease, new techniques for assessing murine liver metabolism are also vital for investigating mechanisms of disease. Alternative methods, such as thermally polarized ^{13}C NMR spectroscopy, are limited by poor sensitivity (20) and ex vivo analysis of blood or urine provides no anatomical information (21). With the advent of DNP technology, high-sensitivity ^{13}C metabolic imaging methods are now more feasible. The findings reported here broaden the scope of DNP to metabolic pathways not previously studied by in vivo imaging modalities. A worthy goal for exploration is the development of DNP-based methodology for the in vivo evaluation of these pathways during the detection and treatment of liver disease in general.

Methods

Sodium [1-^{13}C] pyruvate was obtained from Cambridge Isotopes Laboratory, Inc. and used without further purification. The samples for DNP were

prepared by dissolving the sodium pyruvate into a mixture of 50/50 H_2O/DMSO containing 15 mM trityl radical (i.e., the Tris{8-carboxyl-2,2,6,6-tetra[2-(1-hydroxyethyl)]-benzo(1,2-d:4,5-d)bis(1,3)dithiole-4-yl}methyl sodium salt). The radical was purchased from Oxford Instruments Molecular Biotools Ltd. All other chemicals were purchased from Sigma-Aldrich. C57/bl6 mice were obtained from Charles River Laboratories and given free access to standard mouse chow and water before experiments designated as "fed." Mice for "fasted" experiments were singly housed in fresh cages with H_2O but no food for 24 h before the perfusion experiments. Mice with a liver-specific deletion of pck-1 (cytosolic PEPCK) were generated by crossing pck-1 floxed mice with mice expressing albumin-Cre, as previously described (11).

Perfusions. Protocols for the liver perfusions were approved by the University of Texas Southwestern Medical Center Institutional Animal Care and Use Committee. Following general anesthesia using isoflurane, the livers of adult mice were rapidly excised and perfused through the portal vein, as previously described, with small changes in the available substrates (9). Briefly, the temperature of the liver was held constant at 37 °C and the perfusion was carried out at a constant flow rate of 8 mL/min. The perfusion medium was a Krebs-Henseleit buffer containing 0.2 mM octanoate and 2 mM natural abundance pyruvate. The recirculating medium was filtered and bubbled with a 95/5 mixture of O_2/CO_2. The liver was contained in a 20-mm glass NMR tube. Oxygen consumption measurements were made by measuring the O_2 content in the afferent and efferent perfusate using an ABL80 radiometer. An N of 4 was used for each of the three different liver preparations: fed, fasted, and PEPCK knockout.

DNP and NMR. An Oxford HyperSense DNP system operating at 3.35 T was used to hyperpolarize ~70-μL samples of [1-^{13}C]pyruvate. A total irradiation time of ~90 min yielded a polarization of ~15%. The samples were dissolved with a 4-mL solution of 850 μM Na_2EDTA. After dissolution, 3 mL of the resulting solution was mixed into 20 mL of the perfusate containing the same KH buffer and 0.2 mM octanoate, only to set the pH to 7.4 and provide sufficient oxygenation of the solution. Two perfusion columns were used: one containing KH and a mixture of unpolarized 0.2 mM octanoate and 2 mM pyruvate, and one containing only KH buffer and 0.2 mM octanoate. Column one was switched off and column two was switched on immediately before the HP pyruvate was injected by catheter into the volume directly above the liver. Therefore, the nutrients provided to the liver during the experiment were 0.2 mM octanoate and 2 mM [1-^{13}C]pyruvate. Before

injection of HP pyruvate, manual shimming was performed on the ^{23}Na NMR signal of the perfused liver in a 25-mm NMR tube. ^{13}C NMR spectra were collected using an Agilent VNMRS console equipped with an 89-mm bore 9.4 T magnet and a Doty 25-mm ^{1}H/^{13}C probe. The acquisition scheme used a series of 66° inspection pulses separated by a total acquisition time of 1 s, with no further interpulse delays. No decoupling was used during data acquisition. The 23-mL sample of HP pyruvate was injected by catheter into the perfusion column directly above the liver at a rate of ~19 mL/min. It should be noted that with a flow rate of 8 mL/min for the liver perfusion, this results in a net deposit of material into the column before its flow through the liver. Because this dilution would influence the appearance of the various HP metabolites produced from HP pyruvate, no attempt was made to fit the resulting kinetic curves to obtain rate constants.

In a separate series of experiments, livers were perfused to steady state with 0.2 mM octanoate and 2 mM [U-^{13}C]pyruvate (Cambridge Isotopes), freeze-clamped, acid extracted, and freeze-dried. The resulting powder was dissolved in D_2O for collection of high resolution ^{13}C NMR spectra under complete proton decoupling. An isotopomer analysis was performed on the resulting ^{13}C spectra to determine the relative rates of PDH, TCA cycle flux and anaplerosis (16). These ^{13}C spectra were acquired at 14.1 T using a Agilent VNMRS system (Agilent Inc.) using a 45° pulse and a 2.5-s delay time between pulses. Relative peak areas of each glutamate multiplet were obtained by line fitting in ACD software (Advanced Chemistry Development) and the multiplets were input into the tcaCALC software available through University of Texas Southwestern (17).

Data Processing. Free induction decays obtained from the HP experiment were zero filled to 32,768 points, and the Fourier-transformed peak intensities were measured by integration. For display and analysis of the data, the total area (total carbon signal) of the HP carbon species was obtained by summing the integrated areas of the observed peaks for the time period during which the [1-^{13}C]pyruvate was observed, neglecting the signal associated with the pyruvate hydrate (~179 ppm) and di-pyruvate (~170 ppm) (4). Consequently, the y axes of Figs. 2 and 3 are denoted as the fraction of total carbon signal. For assigning statistical differences between the fractions of total carbon intensity for each metabolite, a two-tailed t test assuming a Gaussian probability distribution was used.

1. Ardenkjaer-Larsen JH, et al. (2003) Increase in signal-to-noise ratio of > 10,000 times in liquid-state NMR. *Proc Natl Acad Sci USA* 100:10158–10163.
2. Chen AP, et al. (2007) Hyperpolarized C-13 spectroscopic imaging of the TRAMP mouse at 3T-initial experience. *Magn Reson Med* 58:1099–1106.
3. Spielman DM, et al. (2009) In vivo measurement of ethanol metabolism in the rat liver using magnetic resonance spectroscopy of hyperpolarized [1-^{13}C]pyruvate. *Magn Reson Med* 62:307–313.
4. Hu S, et al. (2009) In vivo carbon-13 dynamic MRS and MRSI of normal and fasted rat liver with hyperpolarized 13C-pyruvate. *Mol Imaging Biol* 11:399–407.
5. Lau AZ, et al. (2010) Rapid multislice imaging of hyperpolarized ^{13}C pyruvate and bicarbonate in the heart. *Magn Reson Med* 64:1323–1331.
6. Schroeder MA, et al. (2009) Real-time assessment of Krebs cycle metabolism using hyperpolarized ^{13}C magnetic resonance spectroscopy. *FASEB J* 23:2529–2538.
7. Merritt ME, et al. (2007) Hyperpolarized ^{13}C allows a direct measure of flux through a single enzyme-catalyzed step by NMR. *Proc Natl Acad Sci USA* 104:19773–19777.
8. Jones JG, et al. (1997) Measurement of gluconeogenesis and pyruvate recycling in the rat liver: A simple analysis of glucose and glutamate isotopomers during metabolism of [1,2,3-(13)C3]propionate. *FEBS Lett* 412:131–137.
9. Burgess SC, et al. (2004) Impaired tricarboxylic acid cycle activity in mouse livers lacking cytosolic phosphoenolpyruvate carboxykinase. *J Biol Chem* 279:48941–48949.
10. Hausler N, et al. (2006) Effects of insulin and cytosolic redox state on glucose production pathways in the isolated perfused mouse liver measured by integrated ^{2}H and ^{13}C NMR. *Biochem J* 394:465–473.
11. She P, et al. (2000) Phosphoenolpyruvate carboxykinase is necessary for the integration of hepatic energy metabolism. *Mol Cell Biol* 20:6508–6517.
12. Chen AP, et al. (2009) In vivo hyperpolarized ^{13}C MR spectroscopic imaging with ^{1}H decoupling. *J Magn Reson* 197:100–106.
13. Williamson DH, Lund P, Krebs HA (1967) The redox state of free nicotinamide-adenine dinucleotide in the cytoplasm and mitochondria of rat liver. *Biochem J* 103:514–527.
14. Gallagher FA, et al. (2009) Production of hyperpolarized [1,4-^{13}C$_2$]malate from [1,4-^{13}C$_2$]fumarate is a marker of cell necrosis and treatment response in tumors. *Proc Natl Acad Sci USA* 106:19801–19806.
15. Magnusson I, et al. (1991) Noninvasive tracing of Krebs cycle metabolism in liver. *J Biol Chem* 266:6975–6984.
16. Jeffrey FM, Storey CJ, Sherry AD, Malloy CR (1996) ^{13}C isotopomer model for estimation of anaplerotic substrate oxidation via acetyl-CoA. *Am J Physiol* 271:E788–E799.
17. Malloy CR, Sherry AD, Jeffrey FM (1990) Analysis of tricarboxylic acid cycle of the heart using ^{13}C isotope isomers. *Am J Physiol* 259:H987–H995.
18. Cohen SM (1987) 13C NMR study of effects of fasting and diabetes on the metabolism of pyruvate in the tricarboxylic acid cycle and the utilization of pyruvate and ethanol in lipogenesis in perfused rat liver. *Biochemistry* 26:581–589.
19. Yang J, Shen J (2007) Relayed (13)C magnetization transfer: Detection of malate dehydrogenase reaction in vivo. *J Magn Reson* 184:344–349.
20. Rothman DL, Magnusson I, Katz LD, Shulman RG, Shulman GI (1991) Quantitation of hepatic glycogenolysis and gluconeogenesis in fasting humans with 13C NMR. *Science* 254:573–576.
21. Burgess SC, et al. (2003) Noninvasive evaluation of liver metabolism by ^{2}H and ^{13}C NMR isotopomer analysis of human urine. *Anal Biochem* 312:228–234.

APPLIED PHYSICAL SCIENCES

SYSTEMS BIOLOGY

Merritt et al.

www.manaraa.com